Overall Stability Analysis of Enclosed Roadside Noise Barriers

Zhimin Yang[a], Jinhua Tan[b], Youwei Jiang[c*]

School of Transportation and Logistics Engineering, Wuhan University of Technology, WUT, Wuhan, China

[a]yangzhimin@whut.edu.cn,[b]tanjinhua52@gmail.com,
[c*]jiangyouwei304@gmail.com

Abstract. Fully enclosed noise barriers (FENB) have been widely used in urban areas with high-rise buildings, but a new type of enclosed noise barrier with top central opening spaces (TONB) becomes an optimum proposal due to the demand for light transmission and wind resistance. This paper provides a detailed analysis of the overall stability of two enclosed noise barrier samples using the finite element method. The results show that: The combination of deadweight and uneven snow load is most unfavorable for structural buckling stability. The results of buckling coefficients show that TONB has better overall stability than FENB. The influence of geometric nonlinearity and the initial defect cannot be neglected in the calculation of critical buckling load on TONB. The critical buckling load decreases sharply when the initial imperfection increases. The initial imperfection should be minimized during the manufacturing process of TONB.

Keywords: highway engineering; fully enclosed noise barrier; numerical simulation; buckling stability; top opened noise barrier.

1 Introduction

Public health concerns regarding adverse health effects for the population who spend a significant amount of time in high-rise and sound-sensitive buildings near high-traffic roadways have increased substantially in recent years [1-3]. Roadside facilities, including fully enclosed noise barriers(FENB), have been investigated as an effective measure to reduce noise pollution from nearby traffic.

FENB is a system that is commonly made of metal supporting frames and thin acoustic insulation panels. Although FESB has good noise reduction effects [4], it has high costs and poor light transmittance disadvantages. Moreover, the enclosed structure will lead to traffic-induced wind effects and aggravate the adverse influence of wind-snow loads [5].

P. Xiang et al. (eds.), *Proceedings of the 2023 5th International Conference on Hydraulic, Civil and Construction Engineering (HCCE 2023)*, Atlantis Highlights in Engineering 26,
https://doi.org/10.2991/978-94-6463-398-6_76

This paper comes up with an innovative open-top noise barrier (TONB). On TONB, the peak pressures at each section decrease significantly compare to FENB, and the duration of wind loading is shortened [6]. Increasing the opening distance can also promote the dispersion of wind pressure and improve the stress situation [7]. A literature survey shows that the researches on the influence of the top opening space on the stability of noise barriers are still insufficient. Therefore, additional overall stability analysis of TONB is very necessary, and comparing the results with FENB is meaningful.

Buckling eigenvalue is one of the important indexes for the structural overall stability analysis, which includes eigenvalue buckling analysis and nonlinear buckling analysis. Eigenvalue buckling analysis can be used to forecast the theoretical buckling strength of an elastic structure [8,9]. Although the analysis under the ideal condition can get a theoretical result, it is necessary to conduct the nonlinear buckling analysis for better precision [10]. The critical load can be obtained when the structure becomes unstable for the gradually increasing load [11,12]. In this paper, five load combinations are considered to evaluate the overall stability of the noise barriers [13].

2 Methodology

2.1 Linear Buckling

Linear buckling analysis of building structures is a typically generalized eigenvalue problem, which can be used to analyze the buckling stability at the equilibrium bifurcation point for an ideal elastic structure [14-18].

The structure is firstly discretized into a finite number of elements and nodes. The strains and stresses of elements are expressed as the function of the node's displacement according to their geometric and physical relations. The potential energy of the element is figured out by static analysis, and the stiffness matrix and the equivalent point load are obtained. The element stiffness matrix is integrated into the overall stiffness matrix, and the total potential energy of the structure is obtained:

$$\Pi=\frac{1}{2}u^T Ku-u^T F \tag{1}$$

Where K is the overall stiffness matrix, F is the load on the node; u is the displacement of the node. Equation (1) shows that the total potential energy Π of the structure is a function of the node's displacement u. The equilibrium equation is obtained according to the Variational Principle, as in (2):

$$Ku = F \tag{2}$$

From the relation between the buckling deformation and load, it can be concluded that the critical buckling load is the load when the stiffness matrix K is singular. The eigenvalue method has the same principle as the linear buckling analysis, where $K=K_e+ K_\sigma$, K_e is the elastic stiffness matrix and K_σ is the initial stress matrix. The elastic stiffness matrix K_e is derived from the bending-strain potential energy u_b,

which is the function of geometric shape, displacement field, and physical relations, while u_b is not affected by the loads. The initial stress matrix K_σ is derived from the membrane strain potential energy U_m, which is a linear function of the stress and the membrane force.

The following assumptions need to be adopted for both the linear and nonlinear bulking analysis: 1) the deformations of the two samples are elastic and satisfy the Euler-Bernoulli hypothesis, i.e. the cross-section remains plane and perpendicular to the axis during its deformation; 2) the material is linear and elastic. The loading matrix $\overline{F}$ has the same linear relationship as the stress stiffness matrix $\overline{K_\sigma}$ before the structure buckling, as in:

$$\left(K_e + \lambda \overline{K_\sigma}\right) u = \lambda \overline{F} \tag{3}$$

The structure is in a random equilibrium state at the bifurcation point, while the load does not change, and the equilibrium displacement u changes to $u+\delta u$, as in:

$$\left(K_e + \lambda \overline{K_\sigma}\right) u + \delta u = \lambda \overline{F} \tag{4}$$

The difference between (3) and (4) is $\left(K_e + \lambda \overline{K_\sigma}\right) \delta u = 0$. Thus the buckling problem is to find the eigenvalues at the bifurcation point. It needs the equation $\left|K_e + \lambda \overline{K_\sigma}\right| = 0$, then a series of eigenvalue λ and the corresponding δu can be obtained. δu is the deformation pattern when the structure buckles, and is named the buckling mode. The product of the smallest eigenvalue λ and $\overline{F}$ is taken as the critical buckling load. When the acted load is 1, λ is the value of the critical buckling load.

The result of critical buckling load is much greater than the actual failure load. This analysis is to determine the upper limit of the buckling loads, then to analyze the buckling stability using nonlinear theories.

2.2 Nonlinear Buckling

The solution to nonlinear buckling problems includes a series of iterations to establish equilibrium at the new load level [19,20]. The modified Newton-Raphson method evaluates the tangent stiffness matrix at each load step, thus improving the computational efficiency compared to the Newton-Raphson method.

A system of nonlinear equilibrium equation can be written as:

$$\psi(u) = I(u) - f \tag{5}$$

Where $\Psi(u)$ is unbalanced forces, f is the force vector, and internal forces $I(u)$ is defined as:

$$I(u) = \int_v \left[\overline{B}\right] \{\sigma\} dV \tag{6}$$

Where $\{\sigma\}$ is the stress matrix and V is volume. $\left[\overline{B}\right]$ is a strain matrix and could be defined as:

$$\left[\overline{B}\right]\{u\} = \left[B_0\right] + \left[B_L\right]\{u\} \tag{7}$$

Where $\{u\}$ is the displacement vector, $[B_0]$ is the matrix for the linear infinitesimal strain and matrix $[B_L]$ contains the nonlinear strain components.

Unbalance forces $\Psi(u)$ represents the difference between internal and external forces. The basic problem is to find solutions that satisfy the nonlinear equilibrium equation, $\psi(u) = 0$. Since (5) cannot be solved directly for the displacement of u, both an incremental equation of equilibrium from (5) and an iterative procedure are generally used for its solution. The Newton-Raphson method utilizes the first-order approximation of (5) and can be written at load step $n+1$ as:

$$\psi(u_{n+1}^{i+1}) \cong \psi(u_{n+1}^{i}) + \left(\frac{\partial \psi}{\partial u}\right)_{n+1}^{i} \partial u_{n+1}^{i} = 0 \tag{8}$$

Here Vi is the number of iterations, and the tangent stiffness matrix is defined as:

$$\frac{\delta \psi}{\delta u} = \frac{\delta I}{\delta u} = K_T \tag{9}$$

From (8) we have the following iterative correction:

$$K_T^t \partial u_{n+1}^t = -\psi_{n+1}^t \tag{10}$$

where K_T^i is the tangent stiffness matrix at the i^{th} iteration. Thus the improved solution can be computed as:

$$u_{n+1}^{i+1} = u_{n+1}^{i} + \partial u_{n+1}^{i} \tag{11}$$

The modified Newton-Raphson was introduced in which the stiffness matrix is approximated as a constant: $K_T^t \approx \overline{K_t}$ to reduce the burden of computational cost. There are many possible choices of the approximated stiffness matrix $\overline{K_t}$.

3 Numerical Simulation

3.1 Project Overview

Both two samples are symmetrical roadside noise barriers made of portal steel frames, sound-absorbing panels, and Acrylic plates. The left half of TONB is shown in Figure 1. It has an arch-shaped top with rectangular openings. Its sides are installed with vertical panels. The steel supporting frames are bolted at their joints. The total span is 49.5m and the clearance height is 5.0m. The steel supporting frame is made of Q235-

steel and its yield strength is 235MPa. The columns, main beams, and tie beams are made of H-rolled section steel. The thickness of the sound-absorbing panels and Acrylic plates are 95mm and 15mm respectively. The total length is 90m, and the distance between two adjacent portal frames is 3m.

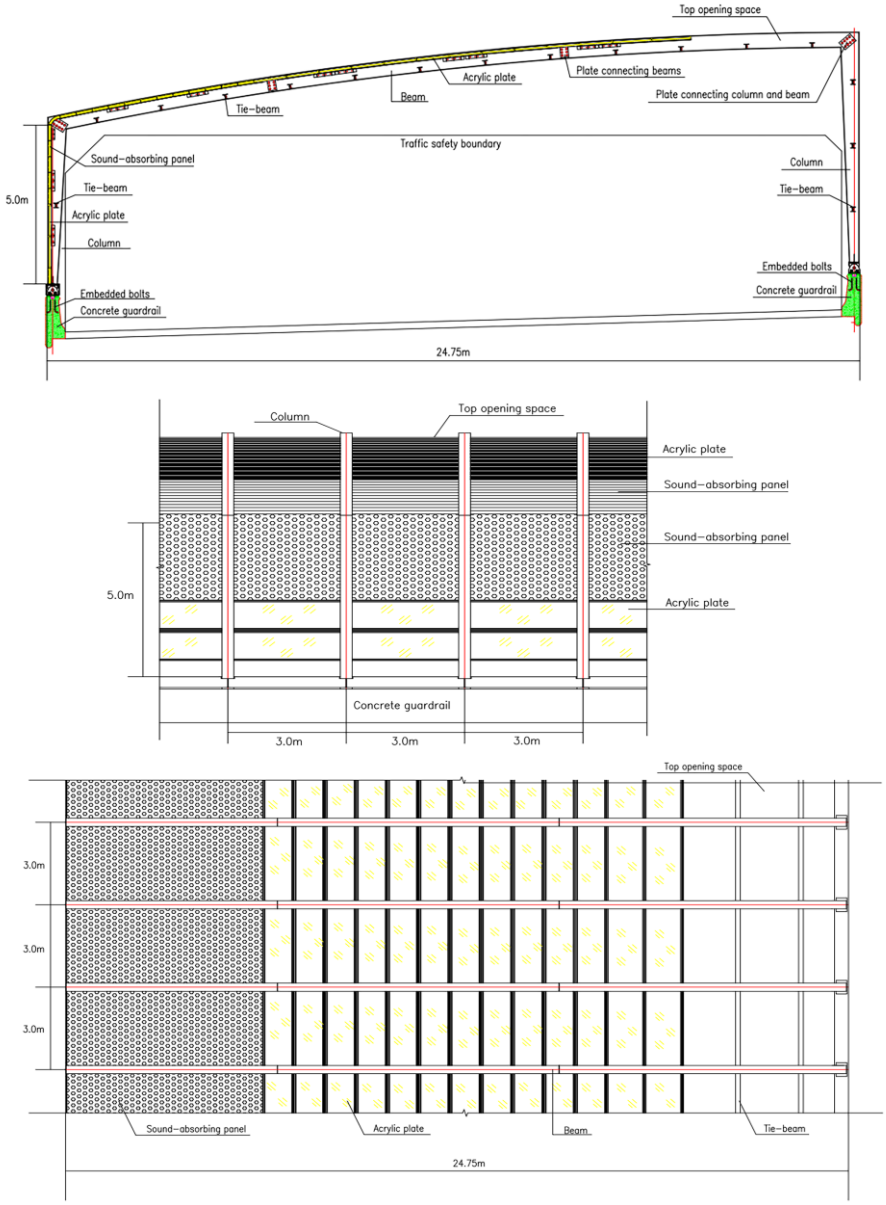

Fig. 1. Three-dimensional views of the left half TONB

3.2 Finite Element Model

Two three-dimensional finite element models are established to conduct the overall stability analysis for the samples. 3D beam elements are used to simulate the steel columns and beams, and shell elements are used to simulate the sound-absorbing panels and Acrylic plates. Rigid constraints are applied at the joints connecting columns and beams, and other contacting places between frames and panels. The basic snow pressure S_0 is 600Pa, and the basic wind pressure ω_0 is 400Pa[21]. The finite element model of TONB/FENB is shown in Figure 2.

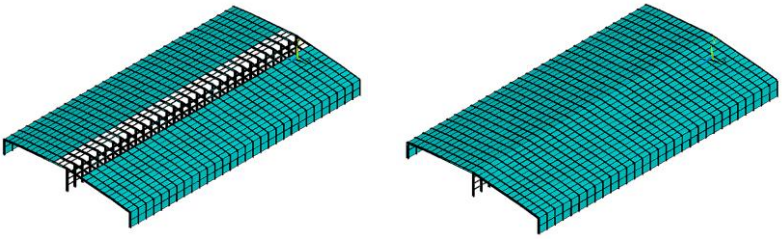

Fig. 2. The TONB/FENB model

4 Overall Stability Analysis

4.1 Eigenvalue Buckling Analysis

The loads on noise barriers mainly include deadweight, wind load, and snow load. The following conditions should be considered for the eigenvalue buckling analysis [22]: (1) Deadweight; (2) Deadweight + wind load; (3) Deadweight + uniform snow load; (4) Deadweight + uneven snow load; (5) Deadweight + wind load + snow load.

During the finite element analysis, the live load is continuously changed to find the limit state when the load buckling coefficient is 1.0 [23], which indicates that the load (dead load + increased live load) is the buckling load of the structure and the increased coefficient is the buckling coefficient of live load. For different load combinations, the first-order eigenvalue is figured out and listed in TABLE I.

Table 1. Buckling Coefficients Under Various Load Conditions

Working Condition	Load Combinations	Live Load Buckling Coefficient(TONB)	Live Load Buckling Coefficient(FENB)
1	Deadweight	159.46	160.59
2	Deadweight and Wind	164.65	178.69
3	Deadweight and Uniform Snow	32.34	25.29
4	Deadweight and Uneven Snow	30.72	24.99
5	Deadweight, Wind, and Snow	32.66	25.59

As can be seen from TABLE I., under the first two load conditions, the live load buckling coefficients are much greater than the other three load conditions. Therefore,

buckling could be ignored in analyzing the overall stability under the first two conditions. Under the last three working conditions, the buckling coefficient of TONB is 27.88%, 22.91%, and 27.66% greater than the buckling coefficient of FENB respectively.

The first-order buckling coefficient under the combination of " Deadweight and uneven snow " is the smallest, such buckling coefficients for TONB and FENB are 30.72 and 24.99 respectively, and both are much greater than 1.0. The critical carrying capacity of TONB is 22.91% higher than FENB, which indicates that TONB has better overall stability than FENB.

Under the action of the fourth load combination, the buckling coefficients and the maximum displacements of the first six order modes for TONB and FENB are shown in TABLE II., and the first four order buckling modes are shown in Figure 3 and Figure 4.

Table 2. The Buckling Stability Coefficients And Maximum Displacements Of The First Six Order Modes

Order Time	TONB		FENB	
	Buckling Stability Coefficient	***Maximum Displacement Ratio***	***Buckling Stability Coefficient***	***Maximum Displacement Ratio***
1	30.72	1.00	24.99	3.87×10^{-3}
2	41.90	0.01	25.65	3.74×10^{-3}
3	42.70	0.03	27.57	5.54×10^{-3}
4	42.81	1.08	30.75	8.34×10^{-3}
5	44.01	0.97	35.13	11.80×10^{-3}
6	45.81	0.01	38.97	21.78×10^{-3}

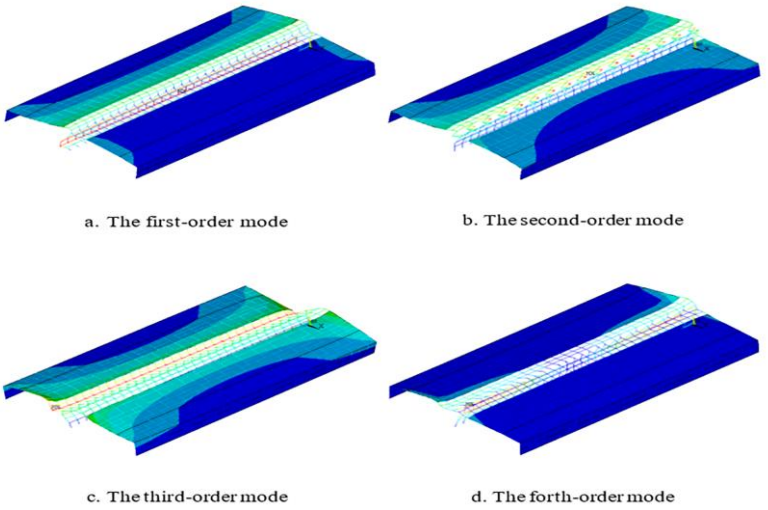

Fig. 3. The first four order buckling modes of TONB

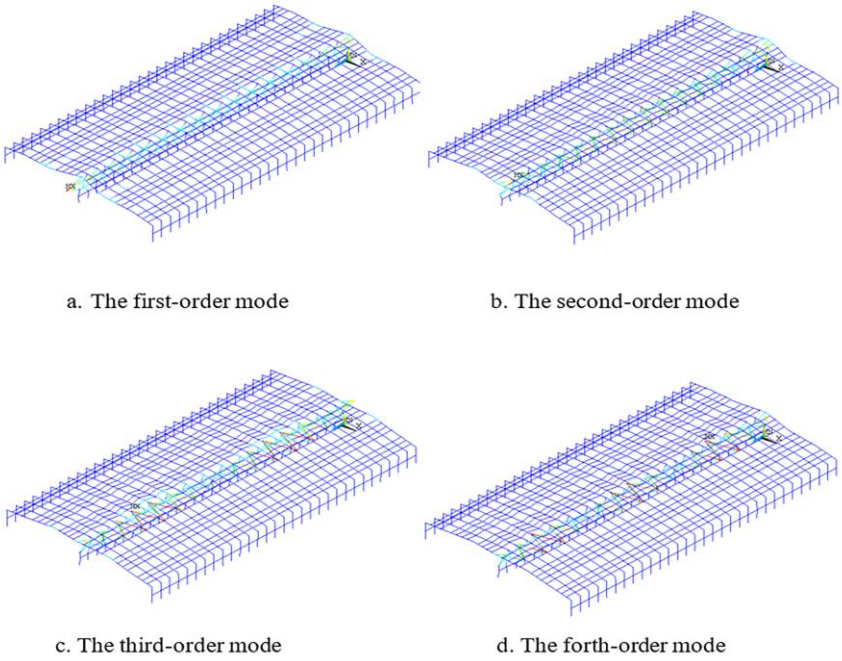

Fig. 4. The first four order buckling modes of FENB (frame only)

As can be seen from Figure 3 and Figure 4, the most vulnerable members are the mid-columns, s beams between the mid-columns, the beams on the windward side, and their tie beams. It can be seen from TABLE II. that the maximum buckling displacement of TONB is much greater than FENB. The critical displacements of the 1st and 4th order of TONB increase 100 times more than FENB, which indicates that the buckling stability and stiffness of TONB are better [24].

4.2 Geometric Nonlinear Buckling Analysis

A geometric nonlinear analysis is carried out with an initial geometric imperfection [25,26] under the load combination of "Deadweight and uneven snow ". The maximum displacement is recorded, and the defection sensitivity of the steel frame is investigated based on the results.

The maximum initial geometric imperfection is 1/N of the beam span L, while N is 100, 200, 500 and 1000 respectively. The load-displacement curves of the maximum displacement node (denoted as point A) are obtained by nonlinear finite element analysis for TONB and FENB, as shown in Figure 5 and Figure 6.

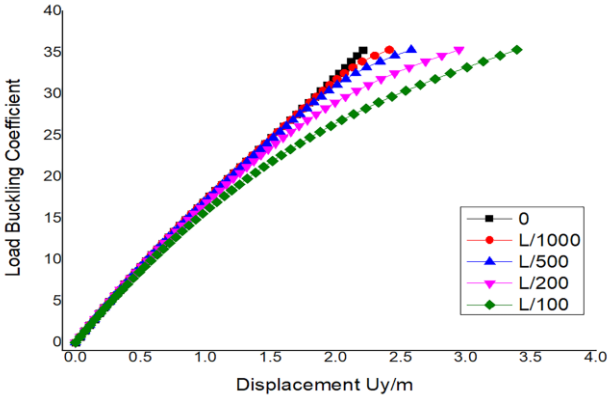

Fig. 5. The load-displacement curve of node A (TONB)

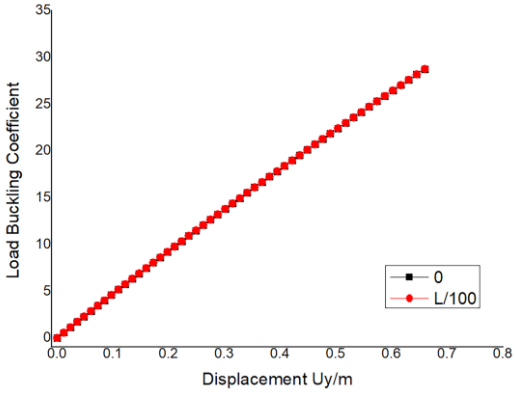

Fig. 6. The load-displacement curve of node A (FENB)

For TONB (Figure 5), the load is small at the beginning, the load-displacement curve is close to linear, and the structure has a large elastic stiffness. The relationship gradually deviates from the line, and the displacement increases more dramatically as the load increases. When the load is close to the critical load, the displacement continues to increase while the load increases very little, and the structure no longer maintains a stable equilibrium state. The buckling coefficient decreases and the vertical critical deformation increases with the increase of initial geometric imperfection.

As can be seen from Figure 6, for FENB, the load-displacement curve of ideal elastic is almost the same as the initial geometric imperfection of L/100, and the buckling coefficients are both around 24.99, which indicates that FENB is insensitive to small initial geometric imperfection.

The geometric nonlinear analysis of TONB is taken under different initial geometric imperfections, the buckling coefficients obtained are shown in TABLE III. When the maximum initial geometric imperfections are L/1000 and L/500, the buckling coefficients are only 1.10% and 3.40% less than the result of the ideal elastic analysis

respectively. When the maximum initial geometric imperfection increases to L/100, the load buckling coefficient is 15.11% less than the result of initial geometric imperfection L/1000, and 16.05% less than the result of the ideal elastic analysis. Initial geometric imperfections have a significant impact on the geometric nonlinear stability of TONB. Therefore, construction precision should be strictly controlled to ensure construction quality and structural safety.

Table 3. Load Buckling Coefficient Of TONB

Initial Geometric Imperfection	0	L/1000	L/500	L/200	L/100
Buckling Coefficient	30.72	30.38	29.68	28.26	25.79

5 Conclusions

The buckling stability and dynamic response under wind-snow load are investigated through the three-dimensional numerical simulation for TONB and FENB respectively:

- The load combination of "Deadweight and uneven snow load" is most unfavorable for structural buckling stability because the buckling coefficient is minimum under this condition, while the eigenvalue buckling coefficient of TONB and FENB are 30.72 and 24.99 respectively.
- The load buckling coefficient of TONB is 22.91% greater than FENB under the most unfavorable condition, which shows that TONB has better overall stability than FENB.
- The geometric nonlinear stability of TONB is highly sensitive to the initial geometric imperfection: When the initial defect is L/100, the load buckling coefficient is 16.05% less than the ideal elastic analysis. Therefore, construction precision should be strictly controlled to ensure construction quality and structural safety.

References

1. Lin D, Sun Z, Shan H, Tang G, Qiu T, Wu M, The Analysis and Countermeasures of Traffic Noise of the Elevated Bridge on the Urban Expressway. Highway,2020,65(04),345-351.
2. Zheng Q, Yang K, Optimized prediction and simulation of traffic noise interference around residents. Computer Simulation,2017,34(11),430-434.
3. Luo P, Cai M, Ma X, Modeling of urban road traffic noise distribution. Environmental Monitoring in China,2013,29(05),176-179.
4. Yin H, Li Y, Gu X, Analysis of noise reduction effect and influencing factors of sound barriers of high-speed railway. China Railway,2009,12,45-46.
5. Zhang G, Cheng W, Liu F, Dang H, Structural design of fully enclosed sound barrier between Beijing Chaoyang Station and the Fifth Ring Road of Beijing-Shenyang high-speed railway. Railway Standard Design,2021,65(06),147-154.

6. Ji X, Zou Y, He X, Huang Y, Jiang S, Influence of top opening space of sound barrier on train-induced wind effect. Journal of Central South University (Science and Technology),2022,53(02),717-726.
7. Wei X, Zhang J, Wei H, Hu Z, Wen Z, Structural effect on the mechanical behavior of high-speed railway sound barriers based on vibration response. Journal of Southwest Jiaotong University,2022,57(02),353-359+409.
8. Zhang X, Study and Analysis on Overall Stability of a Large Span Arch Steel Beam Structure. Shenyang Jianzhu University, 2020.
9. Guo S, Meng Y, Study on the stability of high-pier long-span continuous rigid-frame bridge based on eigenvalue buckling analysis. Urban Roads Bridges & Flood Control,2021,8,275-278+30.
10. Wang Z, Wang X, Zhang F, Zhao Y, Huan J, Jiang X, Nonlinear buckling analysis of Single-layer reticulated shell based on Multi-scale model. Science Technology and Engineering,2022,22(15),6219-6227.
11. Jiang Z, Qiu J, Shi K, Deng Z, Zhong B, Nonlinear buckling analysis of single layer spherical shells with large rise-span ratio. Special Structures, 2022,39(03),87-92.
12. Wang Y, Wang G, Ma L, Hao N, Research on free vibration behavior and nonlinear buckling analysis of Schwedler single-layer latticed shell. Journal of Architecture and Civil Engineering,2013,30(01),104-109.
13. Jiang X, Li W, Guo X, Huang X, Luo P, Zhang M, Analysis of the Full-bridge Mechanical Behavior and Stability of Long-span Special-shaped Arch Bridge, Guangdong Architecture Civil Engineering. 2022,29(06),73-76.
14. Datchanamourty B, Nonlinear static, buckling and dynamic analysis of piezothermoselastic composite plates using reissner-mindlin theory based on a mixed hierarchic finite element formulation. University of Kentucky, 2008.
15. Khazra A, Stress and buckling analysis of grain silos under snow or wind loads. University of Illinois, 1989.
16. Brock J. Development of Modal Analysis for the Study of Global Modes in High-Speed Boundary Layer Flows. University of Minnesota,2017.
17. Dean R.C. On the Asymptotic Reduction of Classical Modal Analysis for Coupled and Nonlinear Dynamical Systems. Duke University,2016.
18. Kong L, Zhang B, Li C, Thermal Buckling and Postbuckling Behaviors of Couple Stress and Surface Energy-Enriched FG-CNTR Nanobeams. Symmetry,2022, 14, 2228.
19. Park O, Buckling and post-buckling analysis of stiffened composite panels in axial compression. University of Florida,1999.
20. Feng Y, Zhang H, Tan X, An T, He Y, Zheng J. Investigation on the buckling and post-buckling performance of aero-stiffened composite panels under axial compression. Polymer Composites,2018, *39(7)*, 2547-2559.
21. Tian Y, Yang Q, Fan C, Proposed revisions on wind load provisions for cladding and components in 'Load code for the design of building structures'. Journal of Building Structures,2017,38(10), 108-115.
22. Liu X, The Dynamic Characteristics Analysis of Large Noise Barrier. Dalian Jiaotong University, 2010.
23. Cao W, Dai G, Fu K, Xiong G, Zhang W, Nie S, Overall stability analysis of steel arch truss of stadium in Lidu new district based on ANSYS. Industrial Construction,2014,44 (S1), 419-423.
24. Huang Z, Liu Z, Xie Y, Buckling analysis of large wind turbine towers. Acta Energiae Solaris Sinica, 2022,43 (04), 304-310.

25. Zhang H, Chen X, Simulation study of initial defects in analysis of overall stability of steel beams. Building Structure,2022,52 (15), 75-79.
26. Salcido, Juan Carlos, Modeling the Effects of Manufacturing Geometric Imperfections in the Buckling Analysis of Three-Dimensional Structures.The University of Texas at El Paso,2017.